



Article

AD-Det: Boosting Object Detection in UAV Images with Focused Small Objects and Balanced Tail Classes

Zhenteng Li ¹, Sheng Lian ^{1,2,3,*} , Dengfeng Pan ¹, Youlin Wang ¹ and Wei Liu ⁴ 

¹ College of Computer and Data Science, Fuzhou University, Fuzhou 350108, China

² Engineering Research Center of Big Data Intelligence, Ministry of Education, Fuzhou 350002, China

³ Key Laboratory of Intelligent Metro of Universities in Fujian, Fuzhou 350108, China

⁴ School of Software and Information Engineering, East China Jiaotong University, Nanchang 330013, China; weiliu@ecjtu.edu.cn

* Correspondence: shenglian@fzu.edu.cn

Abstract: Object detection in unmanned aerial vehicle (UAV) images poses significant challenges due to complex scale variations and class imbalance among objects. Existing methods often address these challenges separately, overlooking the intricate nature of UAV images and the potential synergy between them. In response, this paper proposes AD-Det, a novel framework employing a coherent coarse-to-fine strategy that seamlessly integrates two pivotal components: adaptive small object enhancement (ASOE) and dynamic class-balanced copy-paste (DCC). ASOE utilizes a high-resolution feature map to identify and cluster regions containing small objects. These regions are subsequently enlarged and processed by a fine-grained detector. On the other hand, DCC conducts object-level resampling by dynamically pasting tail classes around the cluster centers obtained by ASOE, maintaining a dynamic memory bank for each tail class. This approach enables AD-Det to not only extract regions with small objects for precise detection but also dynamically perform reasonable resampling for tail-class objects. Consequently, AD-Det enhances the overall detection performance by addressing the challenges of scale variations and class imbalance in UAV images through a synergistic and adaptive framework. We extensively evaluate our approach on two public datasets, i.e., VisDrone and UAVDT, and demonstrate that AD-Det significantly outperforms existing competitive alternatives. Notably, AD-Det achieves a 37.5% average precision (AP) on the VisDrone dataset, surpassing its counterparts by at least 3.1%.

Keywords: object detection; UAV images; scale variations; class imbalance

1. Introduction

Unmanned aerial vehicles (UAVs) have experienced widespread adoption in recent years, driven by their cost-effectiveness and adaptability. Outfitted with cameras and various sensors, UAVs find application in diverse scenarios such as surveillance, rescue operations, agriculture, express delivery, and more. The effectiveness of these applications relies heavily on the seamless and robust recognition of objects within the UAV's field of view, as noted in recent comprehensive reviews [1–3].

Solutions including R-CNN series [4,5], YOLO series [6,7] and, most recently, a query-based series [8–10] have shown leading performance on public datasets such as MS COCO [11]. Despite these accomplishments, when applied to UAV images, particularly for datasets like VisDrone [12], generic detectors' performance falls short of satisfactory in

Academic Editor: Ming-Der Yang

Received: 6 February 2025

Revised: 21 April 2025

Accepted: 25 April 2025

Published: 27 April 2025

Citation: Li, Z.; Lian, S.; Pan, D.; Wang, Y.; Liu, W. AD-Det: Boosting Object Detection in UAV Images with Focused Small Objects and Balanced Tail Classes. *Remote Sens.* **2025**, *17*, 1556. <https://doi.org/10.3390/rs17091556>

Copyright: © 2025 by the authors. Licensee MDPI, Basel, Switzerland. This article is an open access article distributed under the terms and conditions of the Creative Commons Attribution (CC BY) license (<https://creativecommons.org/licenses/by/4.0/>).



terms of accuracy and efficiency. Challenges arise due to hardware limitations, complexities in the imaging environment, and flight trajectory intricacies, leading to the following issues.

Scale variations: Owing to variations in flight altitudes and complex object distribution in UAV images, object sizes differ by distance from camera exposure, exhibiting a broad range of scales, with a predominance of small-scale objects. As illustrated in Figure 1a, within the VisDrone dataset, the proportion of small objects (object size $< 32^2$ pixels) reaches 60.5%, which is 19.1% higher than that in the COCO dataset. On the other hand, the percentage of large objects (object size $> 96^2$ pixels) accounts for only 5.5%. The limited feature representation of small objects poses a considerable challenge, which leads to decreased accuracy and reliability in detecting smaller objects, thus significantly affecting the overall detection performance.

Class imbalance: UAV images collected in urban environments exhibit a long-tailed class imbalance characteristic; a small subset of head classes (e.g., car and people) dominates the dataset, collectively representing over 70% of object instances, while numerous tail classes (e.g., bicycle and van) are severely underrepresented, constituting only 1% to 7% of instances (Figure 1b). This skewed distribution creates a model bias towards head classes during training—detectors prioritize optimizing features for high-frequency categories at the expense of tail classes. Consequently, tail classes suffer from poor localization accuracy and high false-negative rates due to insufficient discriminative feature learning.

To address these challenges, researchers have made many attempts. For scale variations, ref. [13–16] focuses on multi-scale feature fusion, and ref. [17–19] emphasizes hard sample mining. Nevertheless, due to the input scale limitation, there is still room for improvement in accuracy. Another direct method involves cropping the image into subregions before applying detection, such as in uniform cropping. However, these cropping strategies cannot adaptively adjust based on the semantic information in UAV images, potentially including extensive background areas. Li et al. [20] utilize a density map to guide the cropping of images, enhancing the semantics of the resulting subregions. However, this approach involves a density map generation network, which increases model complexity and requires ground truth density map generation. Compared to the scale variations, the challenge of class imbalance is often neglected in UAV images. In recent years, research in the field of long-tailed detection has primarily been categorized into three types: (1) resampling and data augmentation techniques [21]; (2) loss function reweighting methods [17,22]; and (3) decoupled optimization strategies [23]. However, existing approaches still face challenges in dynamically adapting to changes in the distribution of tail classes. Zhang et al. [24] employ a multi-model fusion (MMF) strategy to tackle the head and tail classes distinctly, effectively enhancing the detection performance of tail classes. However, this approach results in the discarding of a substantial amount of valuable data during the training of each model, which could potentially compromise the model's representational capacity.

In this paper, for object detection in UAV images, we propose a novel framework called AD-Det, which adopts a coarse-to-fine strategy and mainly consists of two key components: adaptive small object enhancement (ASOE) and dynamic class-balanced copy-paste (DCC). Specifically, ASOE employs a high-resolution feature map from the classification head to pinpoint small objects. As shown in Figure 1c, most small objects in the image show significant activation in the high-resolution feature map. These positions of interest are clustered into \mathcal{N} subregions, which are then enlarged and processed by a fine-grained detector, thereby enhancing the detection performance of small objects. DCC, on the other hand, performs object-level resampling through a dynamic copy-and-paste strategy specifically tailored for tail-class objects. It leverages the clustering cues from ASOE to dynamically search for suitable pasting positions around the cluster center and maintain a dynamic memory bank for each tail class. Additionally, data augmentation is

conducted to avoid overfitting. In this way, the proposed AD-Det can extract regions with small objects for fine-grained detection and dynamically perform reasonable resampling for tail-class objects, thereby improving overall detection performance.

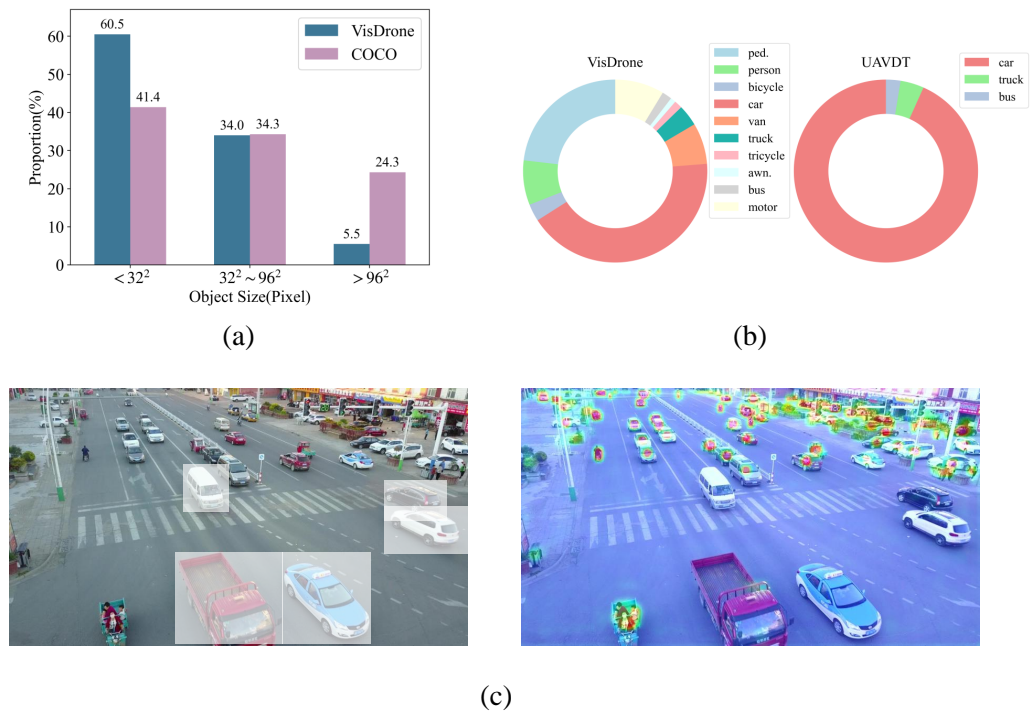


Figure 1. (a) Comparison of scale distribution between VisDrone and COCO. (b) Class distribution of VisDrone and UAVDT. (c) Visualization of high-resolution feature map (P_3) in GFL [25] for VisDrone. It can be seen that the high-resolution feature map mainly focuses on small objects. The masked areas on the left indicate regions that contain large objects, which are easier to handle and can be ignored in the fine-grained detection stage.

Compared to existing coarse-to-fine solutions, our approach is a plug-and-play, unsupervised scheme. The advantages lie in leveraging the inherent properties of the detector to focus on small object regions that truly contribute to accuracy gains, thereby enhancing the precision of small object detection without extra learnable parameters. Additionally, we propose a training-only image augmentation technique for tail classes, which helps to alleviate class imbalance issues.

We summarize four main contributions of this work as follows.

- We propose AD-Det, a novel object detection framework that addresses two key challenges in UAV image object detection—complex scale variations and class imbalance—ultimately enhancing detection performance.
- To enhance small object detection, we propose ASOE, which uses a high-resolution feature map to cluster regions containing small objects, followed by processing them for fine-grained detection.
- To enhance tail-class object detection, we propose DCC, which performs reasonable object-level resampling by dynamically pasting tail classes around clustering centers obtained by ASOE.
- We conduct extensive experiments on VisDrone and UAVDT, which demonstrate that our approach significantly outperforms existing competitive alternatives.

2. Related Works

In object detection tasks, unlike traditional solutions that rely on handcrafted features and classifiers, DL-based solutions can automatically learn discriminative features and achieve promising results. Here, we briefly review object detection solutions in the deep learning era, including (1) generic object detection (in Section 2.1) that focuses on natural images such as MS COCO [11]; (2) object detection in aerial images (in Section 2.2) that focuses on aerial images such as VisDrone [12] and DOTA [26]; and (3) long-tailed object detection (in Section 2.3) that focuses on long-tail scenarios such as LVIS [27].

2.1. Generic Object Detection

Sparked by impressive success in image classification tasks [28], DL-based methods have dominated generic object detection. The existing DL-based detection solutions, when analyzed according to their pipeline, can be roughly grouped into two-stage and one-stage methods. The two-stage detectors are represented by R-CNN [4], Fast R-CNN [29], Faster R-CNN [5], and Mask R-CNN [30]. These detectors first reduce the search space significantly by extracting candidate region proposals. The extracted proposals are then classified into specific categories and refined to proper locations. Such a pipeline leads to relatively higher accuracy but lower efficiency. Different from the above methods, one-stage methods, on the other hand, directly predict objects' categories and locations without region proposals. The representative approaches include the YOLO series [6,7,31], SSD [32], and RetinaNet [17]. Such a design leads to relatively higher efficiency but at the cost of accuracy. Recently, studies into CornerNet [33] and FCOS [34] bypassed the anchor boxes mechanism and corresponding hyperparameter setting and presented promising alternatives for one-stage methods. DETR [35] pioneered a fully end-to-end object detector that employed a transformer-based architecture, eliminating reliance on anchor generation and non-maximum suppression (NMS). Although these detectors achieved impressive progress in generic object detection, their performance on UAV images is far from satisfying due to problems of scale variations and class imbalance.

2.2. Object Detection in Aerial Images

Compared with generic objects that are mostly captured in ground view, object detection in UAV images presents heightened challenges due to object scale and object/category distribution problems.

Many studies focus on **multi-scale/tiny-scale object problems** in aerial images. Most of the early research focuses on the migration of classical generic object detection algorithms. Yang et al. [36] proposed a novel query mechanism, which effectively and efficiently incorporates an additional high-resolution layer to promote small object detection. In the realm of knowledge distillation, Zhu et al. [37] costlessly enhanced the performance of lightweight models by incorporating scale-aware knowledge from more complex ones. To detect small weak objects in UAV images, Han et al. [38] presented a context-scale-aware detector, combining the strengths of context-aware learning and multi-scale feature extraction. Cao et al. [39] introduced a self-reconstructed difference map approach to enhance feature visibility for challenging tiny object detection tasks. DQ-DETR [40] specialized in tiny object detection by employing dynamic query selection and counting-guided feature enhancement, boosting detection performance. SDPDet [41] employed scale-separated dynamic proposals and activation pyramids to enhance the efficiency and accuracy of object detection in UAV views. Zhang et al. [42] enabled detectors to focus on discriminative features while reducing false-positives in cluttered backgrounds. Zhang et al. [43] proposed IMPR-Det, which can integrally mix multi-scale pyramid representations for different components of an instance.

Besides object scale problems, many studies focus on **object/category distribution problems**. Inspired by research into crowd counting, Li et al. [20] injected estimation of density maps into a conventional object detection framework, which was utilized to predict object distribution, reduce the influence of background, and generate more balanced candidate proposals. Duan et al. [44] further adopted a coarse-grained density map to identify subregions more accurately. Similar observations regarding the object distribution issues led [45] to improved RPN in order to cluster region proposals. GLSAN [46] utilized a scale-aware algorithm to fuse global and local detection results. CZDet [47] enhanced cascade detection by innovatively incorporating high-density subregion labels into the repurposed detector. YOLC [48] employed a local scale module and deformable convolutions to enhance accuracy in aerial small object detection. Zhang [49] proposed structured adversarial self-supervised pretraining to strengthen both clean accuracy and adversarial robustness. On the other hand, Yu et al. [50] investigated long-tail category distribution issues, where they designed dedicated samplers and detection heads to address the distinct characteristics of tail and head classes.

Such excellent works have indeed facilitated aerial image object detection. Nevertheless, when addressing scale variations and class imbalance challenges, the majority of preceding studies treat these essential issues rigidly and separately, not only ignoring the complexity of UAV images but also neglecting their potential synergy.

2.3. Long-Tail Object Detection

Much like the paradigm of long-tail classification, research in the domain of long-tail object detection predominantly adheres to two distinctive methodologies: resampling and reweighting. Commonly employed techniques in resampling involve either oversampling the minority classes or undersampling the majority classes during the training process, aimed at mitigating the issue of imbalanced class distribution. Repeat factor sampling (RFS) [27] involves an image-level sampling approach following the resampling paradigm. SimCal [51] proposed a bi-level class balanced sampling approach to alleviate classification head bias. In the context of reweighting, the fundamental concept lies in the assignment of diverse weights to training samples, with a focus on enhancing the training of tail samples. Cui et al. [52] introduced a novel loss function that significantly improves class imbalance handling by dynamically adjusting the weights of training samples based on their effective numbers.

Besides the aforementioned strategies, many researchers have endeavored to handle the long-tail problem from other perspectives. Kang et al. [23] advocated for a decoupled training paradigm that disentangles the learning process into distinct phases: representation learning and classifier training. BAGS [53] grouped classes based on their instance frequency and subsequently applied softmax loss among each group. ROG [54] proposed a multi-task learning approach that concurrently optimizes both object-level classification and global-level score ranking. Hyun et al. [55] introduced effective class-margin loss (ECM) as a novel surrogate objective through which to optimize margin-based binary classification error on the imbalanced training set.

Many earlier coarse-to-fine counterparts pinpoint regions of interest by relying on extra learnable modules or by post-processing sparse boxes. Our method, however, differs by incorporating dense indicators from a high-resolution feature map. This map is adept at preserving extensive information about small objects, facilitating adaptive region generation. Additionally, we enhance this framework by addressing class imbalance issues through the integration of object-level copy-paste techniques. This novel combination effectively tackles two distinct challenges, which are overlooked in existing solutions.

3. Methodology

In this section, we elaborate on the design of AD-Det, including the overall framework of AD-Det in Section 3.1, the ASOE module in Section 3.2, and the DCC module in Section 3.3, along with the training and inference details of AD-Det in Section 3.4.

3.1. Framework Overview

To tackle the key challenges of object detection in UAV images, i.e., scale variations and class imbalance, a novel approach namely AD-Det is proposed. Designed in a coarse-to-fine manner, AD-Det mainly consists of the following two key components. **Adaptive small object enhancement (ASOE)** utilizes the coarse detector cues to roughly locate small objects, and cluster the region of interest for later fine-grained detection. **Dynamic class-balanced copy-paste (DCC)** performs reasonable object-level resampling by dynamically pasting tail classes around the cluster centers obtained by ASOE. The prediction given by the coarse-to-fine strategy is fused through non-maximum suppression (NMS). We illustrate the overall framework of AD-Det in Figure 2.

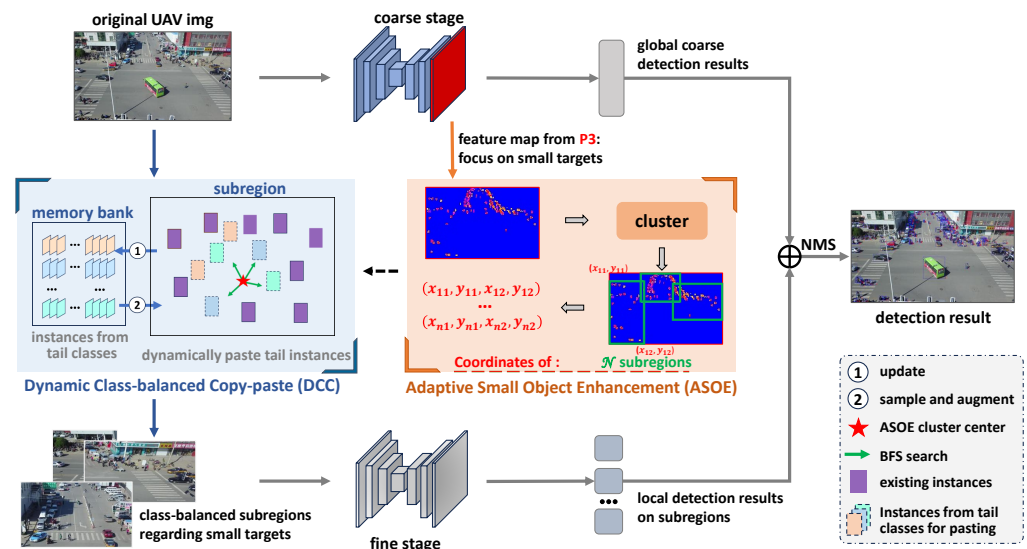


Figure 2. The framework overview of the proposed AD-Det. The network adopts a coarse-to-fine strategy and integrates two key modules, i.e., an adaptive small object enhancement (ASOE) module for excavating regions containing small objects and a dynamic class-balanced copy-paste (DCC) module for balancing class distribution. The final results are obtained by fusing global results and local results using non-maximum suppression (NMS). The dashed line between ASOE and DCC indicates training-only.

3.2. Adaptive Small Object Enhancement (ASOE)

In UAV images, small objects constitute a large proportion and are sparsely distributed (Figure 1a,c), resulting in unsatisfactory detection performance. Such small objects are typically detected from high-resolution low-level feature maps, for example, P_3 in FPN [56]. As shown in Figure 3, the image is passed through the backbone to extract multi-scale features, which are subsequently fused in the FPN. These fused features are then passed to the detection head. Due to varying convolutional strides in different layers, the feature map sizes decrease from P_3 to P_5 . The lower layers, having undergone fewer downsampling operations, not only retain more local information but also have a receptive field better aligned with small objects. As observed from the heatmap comparison, small objects are primarily detected at the P_3 layer. Specifically, the human visual system excels at object detection by quickly scanning the entire image to acquire information on large objects and gain valuable clues in challenging areas with small objects.

Inspired by these factors, we propose adaptive small object enhancement (ASOE), which utilizes a high-resolution feature map to pinpoint regions with small, difficult-to-detect objects for fine-grained detection. Unlike [20], which relies on an additional density network to obtain the position of the foreground object, the proposed ASOE module employs a hierarchical approach, seamlessly integrating coarse-to-fine strategies to overcome the inherent challenges of identifying small objects in UAV images.

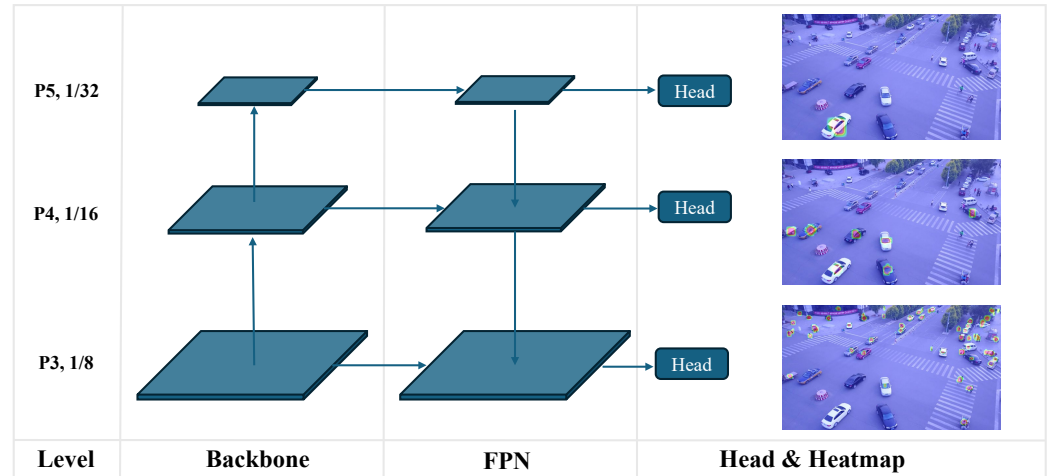


Figure 3. Detector workflow and corresponding heatmap visualizations at different network layers.

In the first stage, a detector $Coarse(\cdot)$ captures the global context and produces preliminary detection results. Meanwhile, the feature map $F_l \in \mathbb{R}^{C \times H \times W}$ (Figure 2 coarse stage red layer), targeting semantic details pertinent to small objects, is extracted from the classification head enriched with high-resolution and low-level features (Figure 3), akin to the methodology employed by RetinaNet [17]. Here, l represents the layer index of P_l , while C , H , and W represent the channel count, height, and width of the feature map. As shown in Figure 4, we compute a position-wise activation map $V_l \in \mathbb{R}^{1 \times H \times W}$ by applying the Sigmoid function independently to each channel of F_l , followed by averaging across channels:

$$V_l = \frac{1}{C} \sum_{c=1}^C \sigma(F_l), \quad (1)$$

where $V_l(i, j)$ indicates the probability of the grid (i, j) containing a small object, and σ is the Sigmoid function. To suppress background noise, we retain only positions where $V_l(i, j)$ exceeds a threshold $\gamma = 0.5$, and by multiplying with the downsampling factor 2^l , these positions can be mapped to the corresponding locations in the original image:

$$T_l = \{(i \times 2^l, j \times 2^l) \mid V_l(i, j) > \gamma\}; \quad (2)$$

these identified positions approximate the small objects' locations, which are prone to being overlooked or inaccurately estimated.

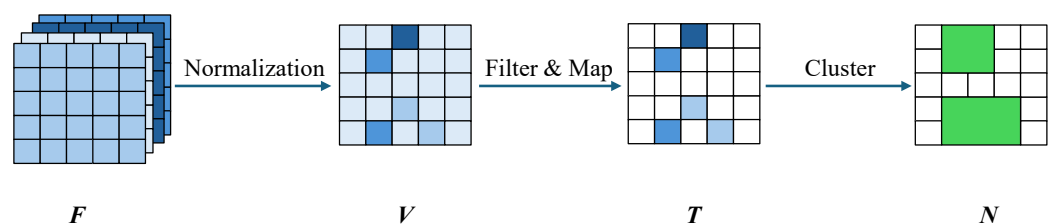


Figure 4. The process of subregion generation in ASOE.

To address the non-uniform distribution of small objects in UAV images, the ASOE module utilizes the K-means algorithm to cluster T_l into \mathcal{N} distinct clusters. The K-means algorithm achieves effective performance gains through K-value optimization, requiring only minimal parameter adaptation for cross-dataset deployment. This balances deterministic region control with adaptability to diverse data distributions, avoiding the parameter sensitivity of DBSCAN and the computational overhead of the mean-shift in real-time UAV applications. The cluster process can be represented as

$$\{C_1, \dots, C_{\mathcal{N}}\} = \text{K-means}(T_l, \mathcal{N}), \quad (3)$$

where $C_k = \{(i, j) \in T_l \mid k = \arg \min_m \|\mathbf{x} - \mu_m\|^2\}$. By determining the top-left and bottom-right coordinates of each cluster, we crop \mathcal{N} subregions from the original image, defined as

$$\{S_i, \dots, S_{\mathcal{N}}\} = \text{CropByTLBR}(C). \quad (4)$$

Subsequently, we upscale the extracted \mathcal{N} subregions and input them into a fine-grained detector, thereby enhancing the detection performance of small objects.

3.3. Dynamic Class-Balanced Copy–Paste (DCC)

To address the challenge of class imbalance in UAV images, resampling techniques like class-balanced sampling and repeat factor sampling are commonly employed. However, these image-level resampling solutions elevate training costs. In contrast, the copy–paste method offers object-level resampling by copying and pasting objects and has shown significantly advanced object detection with ordinary images. However, its application to UAV images has been less effective, which is attributed to their complexity. Therefore, we propose dynamic class-balanced copy–paste (DCC), which differs from traditional copy–paste solutions in considering both the diversity and position rationality of objects.

Firstly, to mitigate overfitting caused by repetitive resampling of specific instances, we introduce a diversity augmentation (DA) strategy, leveraging dynamic memory banks with data augmentation techniques to ensure diverse and balanced training batches. Specifically, each tail class is assigned a memory bank with a capacity of 10 to store instance info:

$$Q = \{\{(x_i, b_i)\}_{i=1}^{10}, \dots, \{(x_i, b_i)\}_{i=1}^{10}\}, \quad (5)$$

where x_i denotes a tail-class instance image, and b_i represents its bounding box coordinates. During training, when the ASOE identifies a subregion S containing small objects, all tail-class instances within this region are enqueued via a first-in-first-out (FIFO) replacement policy:

$$Q = \text{FIFO}(Q, S), \quad (6)$$

where each instance image is cropped with $1.5\times$ bounding box expansion to preserve contextual semantics. Object-level resampling involves strategically pasting tail-class instances into subregions. We first sample an instance (x, b) from Q and then apply data augmentation techniques:

$$(x', b') = \mathcal{A}(x, b), \quad (7)$$

where $\mathcal{A}(\cdot)$ denotes data augmentation techniques such as shift–scale–rotate and random brightness contrast, and (x', b') is the augmented instance for pasting.

Secondly, to make the pasting position more reasonable, we utilize a dynamic search (DS) strategy combined with ASOE clustering cues. Specifically, in ASOE, besides obtaining a subregion S for fine-grained detection, we can also obtain its clustering center (X, Y) , which represents the distribution center of objects in each subregion. The ideal paste position should be closer to the cluster center and maintain no overlap with existing

objects, so DCC dynamically searches a suitable position for (x', b') by performing the BFS algorithm [57] from the cluster center:

$$(X^P, Y^P) = \text{BFS}(S, (X, Y), \text{mask}, b'), \quad (8)$$

$$\text{mask}(i, j) = \begin{cases} 1, & \text{if GT object exists at position } (i, j) \\ 0, & \text{otherwise} \end{cases} \quad \forall i, j \quad (9)$$

where the width and height of b' are employed as the adaptive search step size, and the binary *mask* enables rapid validation of an object's presence in S . Afterward, x' is pasted into the subregion S , and the label set is expanded with b' . Through these operations, we can dynamically and appropriately enhance both the quantity and quality of tail-class instances, effectively balancing their contribution during training.

3.4. Training and Inference Details

In the training process, AD-Det integrates ASOE and DCC to independently train the coarse and fine-grained detectors. To achieve coarse detection and extract the small object feature map, the coarse detector is first trained using all original images, with its training loss function defined as in Equation (10).

$$\mathcal{L}_{\text{coarse}} = \mathcal{L}_{\text{cls}}(x^g, y_{\text{cls}}^g) + \mathcal{L}_{\text{reg}}(x^g, y_{\text{reg}}^g), \quad (10)$$

where \mathcal{L}_{cls} and \mathcal{L}_{reg} denote classification loss and regression loss, and $\{x^g, y^g\}$ denote the original training set. Then, we conduct the coarse detector to traverse the original training set. For each sample, ASOE extracts small object subregions and combines with DCC to augment tail classes. This process yields the fine-grained training set $\{x^l, y^l\}$; the detailed algorithm is illustrated in Algorithm 1, and the training loss function for the fine-grained detector can be represented as Equation (11).

$$\mathcal{L}_{\text{fine}} = \mathcal{L}_{\text{cls}}(x^l, y_{\text{cls}}^l) + \mathcal{L}_{\text{reg}}(x^l, y_{\text{reg}}^l), \quad (11)$$

Algorithm 1: The generation of fine-grained subregions

Input: Normalized high-resolution heatmap V , threshold γ , the number of subregions \mathcal{N} , the state of *Training*

Output: Subregions S

```

1  $Q \leftarrow \{\}$ ;
2  $T \leftarrow \text{Filter}(V, \gamma)$ ;
3 for  $(i, j)$  in  $T$  do
4    $(i, j) \leftarrow (i \times 2^l, j \times 2^l)$ ;
5 end
6  $C_1 \dots C_N \leftarrow \text{Kmeans}(T, \mathcal{N})$ ;
7 for  $C_i$  in  $C$  do
8    $S_i \leftarrow \text{CropByTLBR}(C_i)$ ;
9   if Training is True then
10     $S_i \leftarrow \text{DCC}(S_i, Q)$ ;
11  end
12 end
13  $S \leftarrow \bigcup S_i$ ;
14 return  $S$ ;
```

In the inference process, due to the fine-grained detector's ability to detect subregions with small objects and long-tail distributions, AD-Det exclusively relies on ASOE to acquire related subregions. Let G denote the input UAV image, and the final detection result D_{final} can be formulated as in Equation (12).

$$D_{final} = NMS(Coarse(G), \bigcup_{i=1}^N Fine(S_i)), \quad (12)$$

where $Coarse(\cdot)$ and $Fine(\cdot)$ denote coarse and fine-grained detector, respectively. S_i represents the subregions extracted by ASOE, and NMS stands for non-maximum suppression operation.

4. Experiments

4.1. Experimental Setup

Datasets. We evaluate our AD-Det on two publicly available datasets for UAV image object detection: VisDrone [12] and UAVDT [58]. We summarize the details on these two datasets in Table 1.

VisDrone is a challenging large-scale dataset captured by various camera devices using multiple UAVs. This dataset contains data collected from several Chinese cities, covering different weather conditions and scenarios. Ten predefined categories, including pedestrian, car, van, etc., are manually annotated with bounding boxes. There are 6471 images in the VisDrone for training, complemented by 548 images in the validation set, and a total of 3190 images for testing. The maximal resolution for each image is 2000×1500 pixels. Given that the testing set is not publicly available, we follow ClusDet [45] and DMNet [20] to train the model on the training set while evaluating it on the validation set.

Table 1. Dataset description of VisDrone and UAVDT.

Dataset	Train	Test	Resolution	Classes
VisDrone	6471	548	2000×1500	10
UAVDT	23258	15069	1080×540	3

UAVDT is a large-scale vehicle detection and tracking dataset for UAV scenarios, which is released by UCAS. This dataset contains data collected from complex environments with different weather conditions, occlusion, and flying heights. Bounding boxes have been manually annotated for three predefined categories, including car, truck, and bus. It contains 23,258 and 15,069 images for training and testing, respectively, and the resolution is 1080×540 pixels for each image.

Evaluation metrics. Following the evaluation protocols outlined in MS COCO [11], we employ average precision (AP) as our primary metric, spanning various categories and IoU thresholds. The metrics are succinctly outlined as follows:

- AP: average precision calculated across all categories, considering IoU values within the range of [0.5, 0.95] at intervals of 0.05.
- AP₅₀, AP₇₅: average precision computed across all categories using individual IoU thresholds of 0.5 and 0.75, respectively.
- AP_S, AP_M, AP_L: average precision calculated on object sizes small (less than 32^2), medium (from 32^2 to 96^2), and large (greater than 96^2).

Implementation details. We implement AD-Det using the MMDetection toolbox [59] with PyTorch [60] as the basic framework. The model is trained on a system equipped

with 2*Intel Silver 4210R CPU and 2*NVIDIA A4000 GPU. The baseline detection network employed is GFL [25] with four uniform cropping parts.

Training phase: For the training procedure on VisDrone and UAVDT, as [61] does, the input image size is configured as 1333×800 pixels for VisDrone and 1024×540 pixels for UAVDT, with both coarse and fine-grained detectors. Concerning hyperparameters in the ASOE, the maximum subregion number (N) is set to 4 and 3 on VisDrone and UAVDT, respectively (as discussed in Section 4.4). In the DCC module, all categories except *pedestrian*, *people*, and *car* are considered tail classes on VisDrone, while *truck* and *bus* are considered tail classes on UAVDT. All models undergo 12 epochs of training using an SGD optimizer, with *momentum* = 0.9, *weight decay* = 0.0001, and *initial learning rate* = 0.01. AD-Det is trained with a linear warm-up strategy and undergoes decay by a factor of 10 at epochs 8 and 11.

In the testing phase, the input image size and hyperparameters in the ASOE remain consistent with the training phase unless otherwise specified. In the process of fusing detection, the non-max suppression (NMS) threshold and max detection number are set to 0.5 and 500, respectively, across all datasets.

4.2. Comparison with Representative Solutions

Results on VisDrone. We compare AD-Det with other SOTA solutions on VisDrone, and the results on AP, AP₅₀, and AP₇₅ are listed in Table 2. Our baseline method employs GFL with ResNet-50 / 101, and ResNeXt-101 as backbones. From the table, we have the following observations.

(1) Our proposed method achieves consistent improvement upon all the compared solutions. Our model improves the detection performance to 37.5%, 60.9%, and 39.2% in terms of AP, AP₅₀, and AP₇₅, surpassing all compared methods. Among the compared solutions, ClusDet, DMNet, CDMNet, GLSAN, CZDet, AMRNet, and YOLC employ a coarse-to-fine strategy, which is similar to our approach. Even compared to CZDet, the best solution within them, our model also increases performance by 3.1%, 1.2%, and 4.6% in AP, AP₅₀, and AP₇₅, respectively.

(2) Despite using weaker backbones, our method surpasses or rivals the performance of all compared methods. As illustrated at the bottom of Table 2, although we employed a relatively weak and lightweight backbone ResNet-50, our model continues to be highly competitive. Our method exhibits substantial improvements in AP metrics compared to other methods, even with stronger backbones. For example, compared to YOLC, which used ResNeXt-101 as the backbone, our method, with ResNet-50 as the backbone, nonetheless managed to increase performance by 2.2%, 1.4%, and 3.4% in AP, AP₅₀, and AP₇₅, respectively.

To further evaluate the accuracy and computational complexity of AD-Det, we present a comparison with existing solutions based on AP, parameter counts (Params), floating-point operations (FLOPs), and inference speed (s/img), as shown in Table 3. Under the same backbone architecture of ResNeXt-101, AD-Det demonstrates superior improvements in AP, Params, FLOPs, and inference speed compared to ClusDet, DMNet, and GLSAN. Although our method exhibits marginally higher FLOPs and slightly slower inference speed than CZDet and YOLC, it achieves higher detection accuracy and a significant reduction in Params. These results highlight that our approach delivers competitive performance with a better accuracy–speed trade-off, fulfilling practical engineering requirements for real-world deployment.

Table 2. Comparison of AD-Det with SOTA approaches using AP, AP₅₀, and AP₇₅ on the validation set of VisDrone. The results of comparative experiments are drawn from the corresponding literature. “*” denotes flip augment inference and bold values indicate the best results.

Method	ResNet-50			ResNet-101			ResNeXt-101		
	AP	AP ₅₀	AP ₇₅	AP	AP ₅₀	AP ₇₅	AP	AP ₅₀	AP ₇₅
Faster R-CNN [5]	21.4	40.7	19.9	21.4	40.7	20.3	21.8	41.8	20.1
ClusDet [45]	26.7	50.6	24.7	26.7	50.4	25.2	28.4	53.2	26.4
DMNet [20]	28.2	47.6	28.9	28.5	48.1	29.4	29.4	49.3	30.6
CDMNet [44]	29.2	49.5	29.8	29.7	50.0	30.9	30.7	51.3	32.0
GLSAN [46]	30.7	55.4	30.0	30.7	55.6	29.9	-	-	-
AMRNet [62]	31.7	52.7	33.1	31.7	52.6	33.0	32.1	53.0	33.2
CZDet [47]	33.2	58.3	33.2	34.4	59.7	34.6	-	-	-
YOLC [48]	31.8	55.0	31.7	-	-	-	33.7	57.4	33.8
AD-Det	35.3	57.9	36.6	36.1	58.9	37.6	37.0	60.3	38.3
AD-Det *	35.9	58.8	37.2	36.6	59.7	38.2	37.5	60.9	39.2

Table 3. Comparison of accuracy and complexity with existing solutions using AP, Params, FLOPs, and s/img on the validation set of VisDrone.

Method	Backbone	AP	Params(M)	FLOPs (G)	s/img
ClusDet [45]	ResNeXt-101	28.4	180.95	1647.25	0.759
DMNet [20]	ResNeXt-101	29.4	228.43	4492.18	0.957
GLSAN [46]	ResNet-101	30.7	590.86	2186.76	0.812
CZDet [47]	ResNet-101	34.4	120.32	1329.03	0.593
YOLC [48]	ResNeXt-101	33.7	125.32	1245.25	0.657
AD-Det	ResNet-50	35.3	64.10	1072.05	0.514
	ResNet-101	36.1	102.10	1471.40	0.615
	ResNeXt-101	37.0	101.36	1491.00	0.701

Results on UAVDT. Similar situations occur when our method is evaluated on UAVDT, and the detection accuracy compared with SOTA methods on the testing set of UAVDT is shown in Table 4. To facilitate comparison, we utilize GFL with ResNet-50 backbone as our baseline. Compared with other SOTA methods, our method attains a new SOTA performance even with relatively weaker ResNet-50 as the backbone, achieving 20.1% in AP, 34.2% in AP₅₀, and 21.9% in AP₇₅. In comparison with the GLSAN, our model demonstrates increases of 3.1%, 6.1%, and 3.1% in AP, AP₅₀, and AP₇₅, respectively.

Table 4. Comparison of AD-Det with SOTA approaches using AP, AP₅₀, and AP₇₅ on the testing set of UAVDT. The results of comparative experiments are drawn from the corresponding literature. The best results are highlighted in bold.

Method	Backbone	AP	AP ₅₀	AP ₇₅
Faster R-CNN [5]	ResNet-50	11.0	23.4	8.4
ClusDet [45]	ResNet-50	13.7	26.5	12.5
DMNet [20]	ResNet-50	14.7	24.6	16.3
CDMNet [44]	ResNet-50	16.8	29.1	18.5
GLSAN [46]	ResNet-50	17.0	28.1	18.8
AMRNet [62]	ResNet-50	18.2	30.4	19.8
CZDet [47]	ResNet-50	18.9	30.2	20.3
YOLC [48]	HRNet	19.3	30.9	20.1
AD-Det	ResNet-50	20.1	34.2	21.9

4.3. Qualitative Analysis

To qualitatively contrast the performance, Figure 5 depicts the detection results for both the baseline detector and our AD-Det. It is evident that our method surpasses the baseline detector and reaches a satisfactory detection accuracy. Specifically, as depicted in the dashed area of Figure 5 and the corresponding zoom-in views, our approach excels in detecting small objects and tail categories. This superiority can be attributed to the contributions of ASOE and DCC, which collectively enhance UAV image object detection from two distinct perspectives.

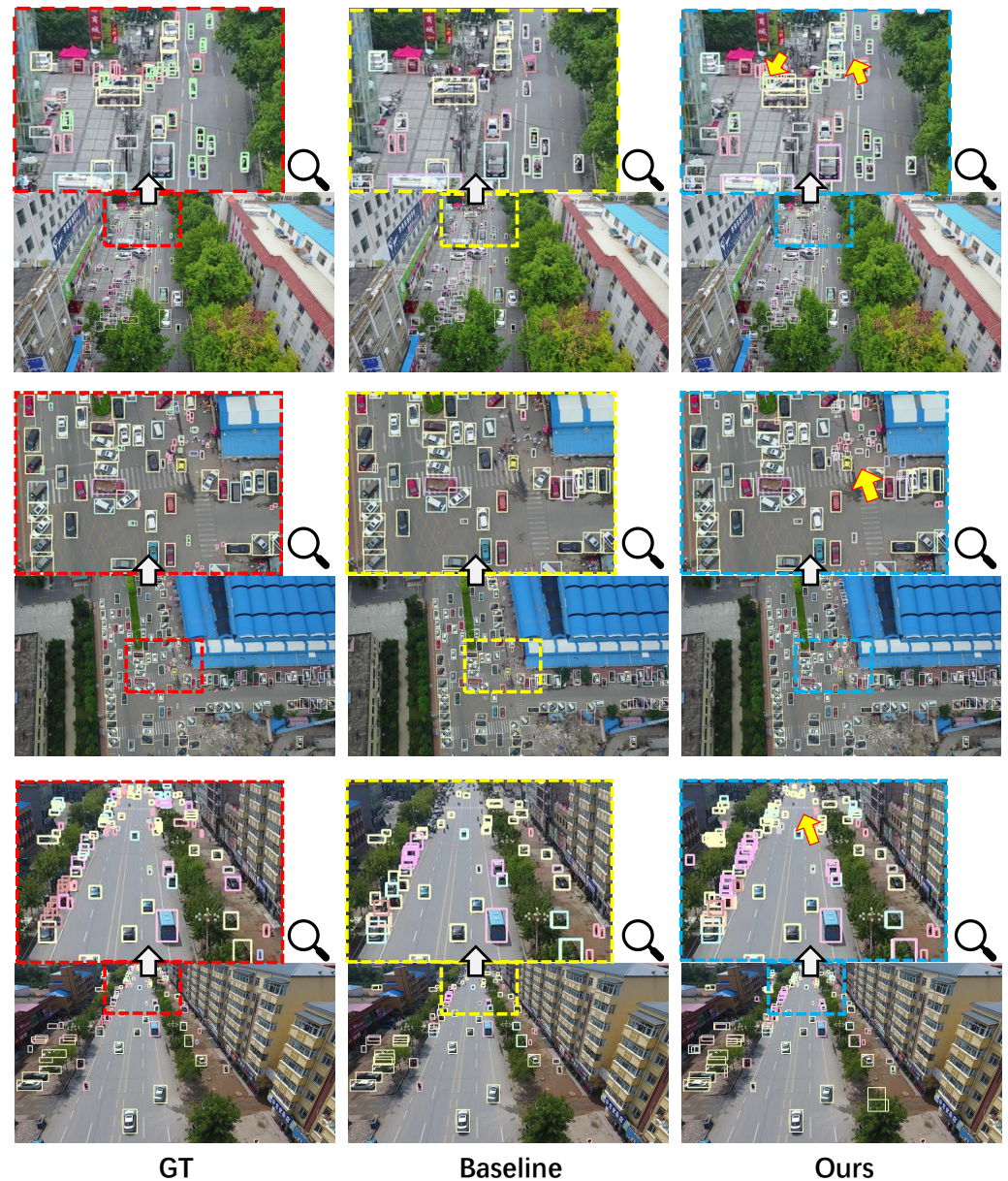


Figure 5. Visualization of qualitative comparison between the baseline detector and our proposed method on VisDrone. The areas marked by the dashed boxes indicate that our approach excels in detecting small objects and tail categories.

4.4. Ablation Study

We conduct extensive studies on VisDrone to validate the effectiveness of our key design, including (1) the effectiveness of ASOE and DCC modules, (2) the choice of key hyperparameters, (3) the selection of the base detector, (4) the design of the ASOE module,

and (5) the design of the DCC module. For all ablation studies, we employ ResNet-50 as our backbone.

The effectiveness of ASOE and DCC modules: As the key components of our method, ASOE and DCC are systematically incorporated into the model to evaluate their respective efficacies. Simultaneously, we demonstrate the improvements resulting from the integration of ASOE and DCC, emphasizing their mutual complementarity. A comprehensive presentation of the ablation study is provided in Table 5 and Figure 6, which illustrate the accuracy improvements across different metrics after integrating our key components.

Table 5. The impacts of the proposed modules on detection performance in VisDrone. ASOE and DCC indicate our proposed adaptive small object enhancement and dynamic class-balanced copy–paste method. The best results are highlighted in bold.

Method	AP	AP_50	AP_75	AP_S	AP_M	AP_L	s/img
Baseline	33.1	55.0	34.0	24.3	44.1	44.9	0.706
Baseline + ASOE	35.3	58.0	36.5	27.5	44.8	45.4	0.758
Baseline + ASOE + DCC	35.9	58.8	37.2	28.0	45.7	45.2	0.758

As illustrated in Table 5, the incorporation of ASOE results in a notable improvement of 2.2% in AP and 3.0% in AP_S over the baseline method. Similarly, DCC contributes to an enhancement in detection performance, elevating it from 35.3% to 35.9% in AP. Compared to baseline with identical parameter settings, our method achieves a notable increase in accuracy, but only increases time consumption slightly.

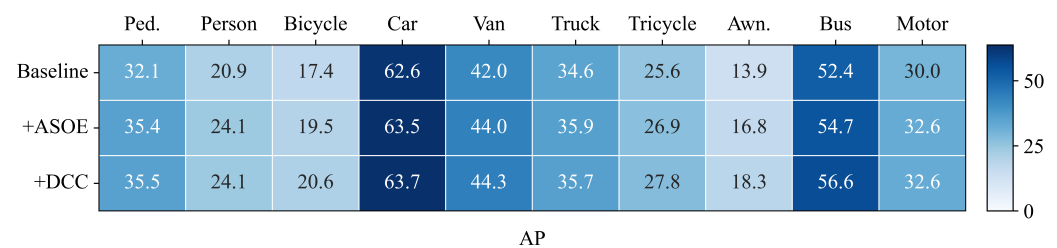


Figure 6. Ablation for ten fine-grained categories with AP. Ped. and Awn. denote Pedestrian and Awning-tricycle. ASOE and DCC indicate our proposed adaptive small object enhancement and dynamic class-balanced copy–paste method.

As illustrated in Figure 6, a noteworthy observation is the consistent enhancement in results for objects in the tail categories, especially for *bicycles*, *tricycles*, *awn.*, and *buses*, which improved by 0.9%~1.9%, underscoring the ability of DCC to augment detection performance reliably. Significantly, the addition of complementary samples through DCC does not adversely affect the performance of other categories.

The choice of key hyperparameters: We analyze the impact of two key hyperparameters herein—the number of subregions \mathcal{N} in Figure 7a and the confidence threshold γ in Figure 7b.

The number of subregions \mathcal{N} is a pivotal parameter that significantly influences the detection speed and accuracy. The effects of different values of \mathcal{N} on detection time and accuracy are summarized in Figure 7a. This subfigure indicates that as the number of subregions increases, the network’s detection accuracy improves, but with an associated increase in detection time. Considering the trade-off between accuracy and efficiency, this study selects $\mathcal{N} = 4$ as the optimal number of subregions. We conduct a similar experiment on UAVDT and find that $\mathcal{N} = 3$ is the optimal choice for UAVDT.

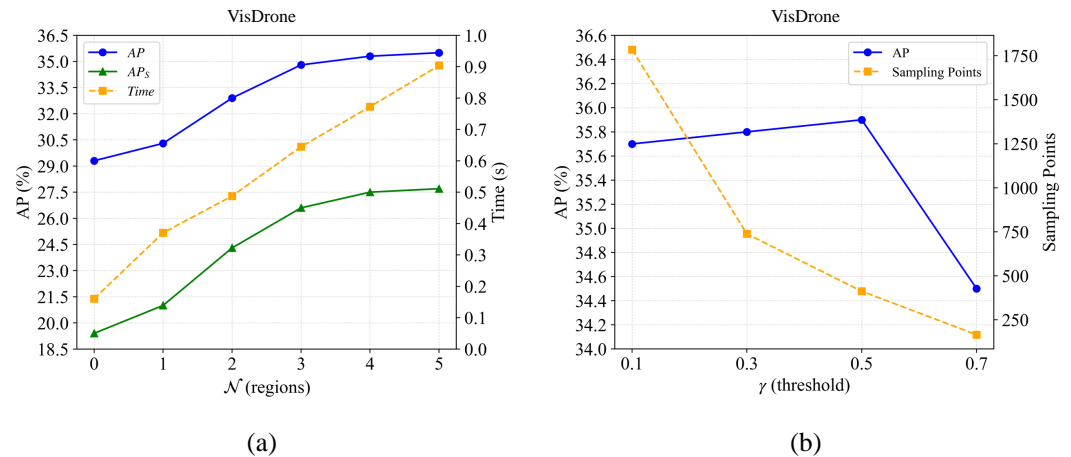


Figure 7. (a) AP, AP_S and inference time curves on different numbers of subregions N on the validation set of VisDrone. (b) AP and sample point curves on different confidence thresholds' γ values in Equation (2) on the validation set of VisDrone. The sample points denote the points utilized for clustering in ASOE.

The confidence threshold γ determines the quality of the subregions (Equation (2)). We experiment with different γ values in {0.1, 0.3, 0.5, 0.7}. In particular, we quantify sample points and their corresponding detection accuracy. As depicted in Figure 7b, with an increase in γ , the number of sample points decreases, facilitating a proportional acceleration in clustering speed. However, the accuracy benefits are not linear with higher γ values. When $\gamma = 0.7$, an excessive number of points are disregarded, leading to a significant decline in detection accuracy. Therefore, we select $\gamma = 0.5$ as the threshold parameter.

The selection of a base detector: In Table 6, we present a comparison of GFL with several leading base detectors, where GFL achieves superior performance. As indicated by AP_S , both GFL and CenterNet are effective in small object detection, but GFL exhibits more balanced accuracy across various object scales. In contrast to FCOS and YOLOv8, GFL outperforms both in AP and AP_S . Therefore, we choose GFL as the base detector of AD-Det.

Table 6. Comparison of GFL with leading base detectors. The best results are highlighted in bold.

Method	AP	AP_50	AP_75	AP_S	AP_M	AP_L
FCOS [34]	26.7	45.2	27.1	17.4	38.8	45.1
CenterNet [63]	27.2	49.8	25.8	19.4	38.7	39.2
YoloV8 [7]	26.1	43.9	26.4	15.8	39.2	52.1
GFL [25]	29.3	48.2	30.2	19.4	42.1	45.2

The design of the ASOE module: In our ASOE module, we empirically select the lowest layer of the feature maps, namely P_3 , as our primary focus [56]. In Figure 8, we visualize the regions of interest selected by ASOE using different feature maps. The visualization shows that the P_3 layer focuses more on small object regions, while higher layers such as P_4 and P_5 gradually focus on larger objects. To substantiate its efficacy, we conduct a straightforward comparison with the higher adjacent layer P_4 as an alternative focus. We summarize the results in Table 7. Experimental results indicate that the P_3 layer yields the highest performance, while clustering from higher-level layers such as P_4 would lead to performance degradation. Note that AP and AP_S undergo a sharp decrease from P_3 to P_4 , highlighting our approach's effectiveness in detecting small objects within higher-resolution layers.

The design of the DCC module: DCC comprises two major components—diversity augmentation (DA) and dynamic search (DS). Based on ASOE, we verify these two components step by step. As shown in Table 8, when DA is applied to tail-class instances, the AP_S and AP_M are increased by 0.4% and 0.7%, respectively. When further combined with DS, the AP is increased to 35.9%, which proves its effectiveness.

Table 7. Ablation for our ASOE module. P_3 denotes the lowest layer of the feature maps, and P_4 is the higher adjacent layer. The best results are highlighted in bold.

Method	AP	AP_50	AP_75	AP_S	AP_M	AP_L
Baseline	33.1	55.0	34.0	24.3	44.1	44.9
with P_4	30.4	50.9	30.9	21.3	42.2	45.4
with P_3 (ours)	35.3	58.0	36.5	27.5	44.8	45.4

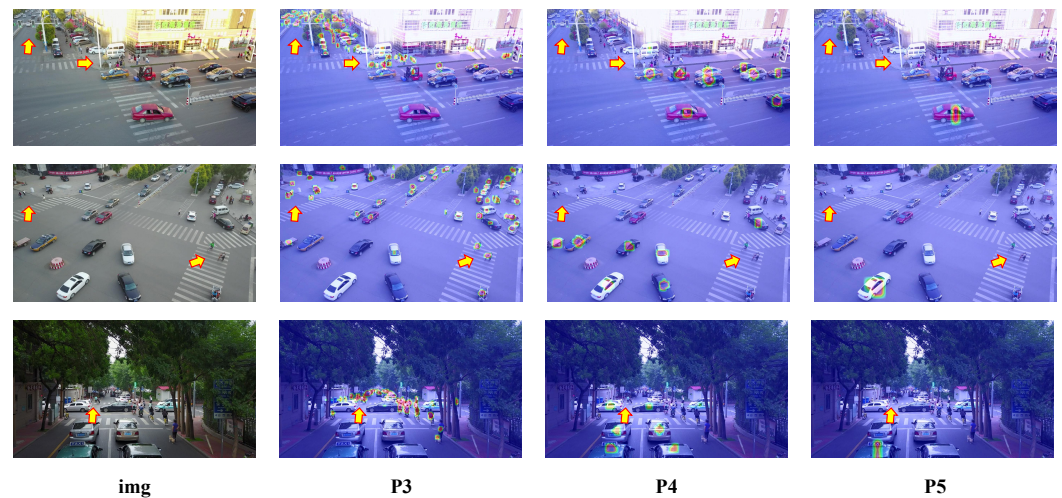


Figure 8. Visualization of interesting regions selected by ASOE using different feature maps. Arrows point to small objects.

Table 8. Ablation for our DCC module. DA and DS indicate diversity augmentation for tail classes and dynamic position search for tail classes, respectively. The best results are highlighted in bold.

Method	AP	AP_50	AP_75	AP_S	AP_M	AP_L
ASOE	35.3	58.0	36.5	27.5	44.8	45.4
ASOE + DA	35.6	58.5	36.9	27.9	45.5	45.3
ASOE + DA + DS	35.9	58.8	37.2	28.0	45.7	45.2

5. Conclusions

In this paper, we propose AD-Det, a novel object detection framework for UAV images, which addresses the challenges of scale variations and class imbalance. AD-Det consists of two key components: adaptive small object enhancement (ASOE) and dynamic class-balanced copy-paste (DCC). ASOE employs a high-resolution feature map to cluster regions containing small objects, followed by processing them for fine-grained detection. DCC performs reasonable object resampling by dynamically pasting tail classes around clustering centers obtained by ASOE. We conduct extensive experiments on VisDrone and UAVDT and demonstrate that our approach significantly outperforms existing competitive alternatives.

Although our proposed approach achieves satisfactory results in UAV image object detection, several limitations remain to be addressed in our future endeavors. (1) ASOE achieves precise detection of small objects by leveraging global location cues, but the usage of global features is still limited. ASOE ignores the feature interaction between

the global image and the local regions, which may help to better understand the scene's semantic knowledge. (2) DCC conducts uniform sampling copy–paste, but there is room for improvement by considering instance-specific metrics and the complex relationships between classes for more effective hard example mining. In the future, we plan to explore more effective ways of handling UAV images under complex scenarios, including occlusion and background clutter issues.

Author Contributions: Conceptualization, Z.L. and S.L.; methodology, Z.L.; software, D.P. and Y.W.; validation, Z.L., S.L. and D.P.; formal analysis, Z.L. and S.L.; investigation, Z.L. and Y.W.; resources, Z.L.; data curation, Z.L.; writing—original draft preparation, Z.L. and S.L.; writing—review and editing, S.L. and W.L.; visualization, Z.L.; supervision, S.L. All authors have read and agreed to the published version of the manuscript.

Funding: This research was funded by the Natural Science Foundation of Fujian Province of China youth project (No. 2023J05117); the Education and Scientific Research Project for Middle-aged and Young Teachers in Fujian Province (No. JAT220017); the National Natural Science Foundation of China (No. 62461026); and the Natural Science Foundation of Jiangxi Province (No. 20232BAB203057).

Data Availability Statement: The datasets used in this study are all open-source: VisDrone is available at <https://github.com/VisDrone/VisDrone-Dataset> (accessed on 17 January 2025), and UAVDT can be accessed at <https://sites.google.com/view/grli-uavdt> (accessed on 17 January 2025).

Conflicts of Interest: The authors declare no conflicts of interest.

References

1. Osco, L.P.; Junior, J.M.; Ramos, A.P.M.; de Castro Jorge, L.A.; Fatholahi, S.N.; de Andrade Silva, J.; Matsubara, E.T.; Pistori, H.; Gonçalves, W.N.; Li, J. A review on deep learning in UAV remote sensing. *Int. J. Appl. Earth Obs. Geoinf.* **2021**, *102*, 102456. [CrossRef]
2. Zuo, Z.; Liu, C.; Han, Q.L.; Song, J. Unmanned aerial vehicles: Control methods and future challenges. *IEEE/CAA J. Autom. Sin.* **2022**, *9*, 601–614. [CrossRef]
3. Kurunathan, H.; Huang, H.; Li, K.; Ni, W.; Hossain, E. Machine Learning-Aided Operations and Communications of Unmanned Aerial Vehicles: A Contemporary Survey. *IEEE Commun. Surv. Tutor.* **2024**, *26*, 496–533. [CrossRef]
4. Girshick, R.; Donahue, J.; Darrell, T.; Malik, J. Rich Feature Hierarchies for Accurate Object Detection and Semantic Segmentation. In Proceedings of the IEEE International Conference on Computer Vision and Pattern Recognition, Columbus, OH, USA, 23–28 June 2014.
5. Ren, S.; He, K.; Girshick, R.; Sun, J. Faster r-cnn: Towards real-time object detection with region proposal networks. In Proceedings of the Advances in Neural Information Processing Systems, Montreal, QC, Canada, 7–12 December 2015.
6. Redmon, J.; Divvala, S.; Girshick, R.; Farhadi, A. You only look once: Unified, real-time object detection. In Proceedings of the IEEE International Conference on Computer Vision and Pattern Recognition, Las Vegas, NV, USA, 27–30 June 2016.
7. Wang, C.Y.; Bochkovskiy, A.; Liao, H.Y.M. YOLOv7: Trainable bag-of-freebies sets new state-of-the-art for real-time object detectors. In Proceedings of the IEEE International Conference on Computer Vision and Pattern Recognition, Vancouver, BC, Canada, 17–24 June 2023.
8. Gao, Z.; Wang, L.; Han, B.; Guo, S. Adamixer: A fast-converging query-based object detector. In Proceedings of the IEEE International Conference on Computer Vision and Pattern Recognition, New Orleans, LA, USA, 18–24 June 2022.
9. Li, Y.; Wang, S. R(Det)2: Randomized Decision Routing for Object Detection. In Proceedings of the IEEE International Conference on Computer Vision and Pattern Recognition, New Orleans, LA, USA, 18–24 June 2022.
10. Jia, D.; Yuan, Y.; He, H.; Wu, X.; Yu, H.; Lin, W.; Sun, L.; Zhang, C.; Hu, H. DETRs With Hybrid Matching. In Proceedings of the IEEE International Conference on Computer Vision and Pattern Recognition, Vancouver, BC, Canada, 17–24 June 2023.
11. Lin, T.Y.; Maire, M.; Belongie, S.; Hays, J.; Perona, P.; Ramanan, D.; Dollár, P.; Zitnick, C.L. Microsoft COCO: Common Objects in Context. In Proceedings of the European Conference on Computer Vision, Zurich, Switzerland, 6–12 September 2014.
12. Zhu, P.; Wen, L.; Du, D.; Bian, X.; Fan, H.; Hu, Q.; Ling, H. Detection and tracking meet drones challenge. *IEEE Trans. Pattern Anal. Mach. Intell.* **2021**, *44*, 7380–7399. [CrossRef]
13. Gao, T.; Niu, Q.; Zhang, J.; Chen, T.; Mei, S.; Jubair, A. Global to local: A scale-aware network for remote sensing object detection. *IEEE Trans. Geosci. Remote Sens.* **2023**, *61*, 1–14. [CrossRef]
14. Chen, Z.; Ji, H.; Zhang, Y.; Zhu, Z.; Li, Y. High-resolution feature pyramid network for small object detection on drone view. *IEEE Trans. Circuits Syst. Video Technol.* **2023**, *34*, 475–489. [CrossRef]

15. Liu, W.; Kang, Z.; Liu, J.; Lin, Y.; Yu, Y.; Li, J. A Multitask CNN-Transformer Network for Semantic Change Detection From Bi-temporal Remote Sensing Images. *IEEE Trans. Geosci. Remote Sens.* **2024**.
16. Liu, W.; Lin, Y.; Liu, W.; Yu, Y.; Li, J. An attention-based multiscale transformer network for remote sensing image change detection. *ISPRS J. Photogramm. Remote Sens.* **2023**, *202*, 599–609. [[CrossRef](#)]
17. Lin, T.Y.; Goyal, P.; Girshick, R.; He, K.; Dollár, P. Focal loss for dense object detection. In Proceedings of the IEEE International Conference on Computer Vision, Venice, Italy, 22–29 October 2017.
18. Biswas, D.; Tešić, J. Small object difficulty (sod) modeling for objects detection in satellite images. In Proceedings of the International Conference on Computational Intelligence and Communication Networks, Al-Khobar, Saudi Arabia, 4–6 December 2022.
19. Biswas, D.; Tešić, J. Unsupervised domain adaptation with debiased contrastive learning and support-set guided pseudo labeling for remote sensing images. *IEEE J. Sel. Top. Appl. Earth Obs. Remote Sens.* **2024**, *17*, 3197–3210. [[CrossRef](#)]
20. Li, C.; Yang, T.; Zhu, S.; Chen, C.; Guan, S. Density Map Guided Object Detection in Aerial Images. In Proceedings of the IEEE International Conference on Computer Vision and Pattern Recognition Workshops, Seattle, WA, USA, 14–19 June 2020.
21. Ghiasi, G.; Cui, Y.; Srinivas, A.; Qian, R.; Lin, T.Y.; Cubuk, E.D.; Le, Q.V.; Zoph, B. Simple Copy-Paste Is a Strong Data Augmentation Method for Instance Segmentation. In Proceedings of the IEEE International Conference on Computer Vision and Pattern Recognition, Nashville, TN, USA, 20–25 June 2021.
22. Li, B.; Liu, Y.; Wang, X. Gradient Harmonized Single-Stage Detector. *Proc. AAAI Conf. Artif. Intell.* **2019**, *33*, 8577–8584. [[CrossRef](#)]
23. Kang, B.; Xie, S.; Rohrbach, M.; Yan, Z.; Gordo, A.; Feng, J.; Kalantidis, Y. Decoupling representation and classifier for long-tailed recognition. *arXiv* **2019**, arXiv:1910.09217.
24. Zhang, X.; Izquierdo, E.; Chandramouli, K. Dense and Small Object Detection in UAV Vision Based on Cascade Network. In Proceedings of the IEEE International Conference on Computer Vision Workshops, Seoul, Republic of Korea, 27–28 October 2019.
25. Li, X.; Wang, W.; Wu, L.; Chen, S.; Hu, X.; Li, J.; Tang, J.; Yang, J. Generalized Focal Loss: Learning Qualified and Distributed Bounding Boxes for Dense Object Detection. In Proceedings of the Advances in Neural Information Processing Systems, Virtual, 6–12 December 2020.
26. Ding, J.; Xue, N.; Xia, G.S.; Bai, X.; Yang, W.; Yang, M.; Belongie, S.; Luo, J.; Datcu, M.; Pelillo, M.; et al. Object Detection in Aerial Images: A Large-Scale Benchmark and Challenges. *IEEE Trans. Pattern Anal. Mach. Intell.* **2021**, *44*, 7778–7796. [[CrossRef](#)] [[PubMed](#)]
27. Gupta, A.; Dollar, P.; Girshick, R. Lvis: A dataset for large vocabulary instance segmentation. In Proceedings of the IEEE International Conference on Computer Vision and Pattern Recognition, Long Beach, CA, USA, 15–20 June 2019.
28. Krizhevsky, A.; Sutskever, I.; Hinton, G.E. Imagenet classification with deep convolutional neural networks. *Commun. ACM* **2017**, *60*, 84–90. [[CrossRef](#)]
29. Girshick, R. Fast r-cnn. In Proceedings of the IEEE International Conference on Computer Vision, Santiago, Chile, 7–13 December 2015.
30. He, K.; Gkioxari, G.; Dollár, P.; Girshick, R. Mask r-cnn. In Proceedings of the IEEE International Conference on Computer Vision, Venice, Italy, 22–29 October 2017.
31. Redmon, J.; Farhadi, A. YOLO9000: Better, faster, stronger. In Proceedings of the IEEE International Conference on Computer Vision and Pattern Recognition, Honolulu, HI, USA, 21–26 July 2017.
32. Liu, W.; Anguelov, D.; Erhan, D.; Szegedy, C.; Reed, S.; Fu, C.Y.; Berg, A.C. Ssd: Single shot multibox detector. In Proceedings of the European Conference on Computer Vision, Amsterdam, The Netherlands, 11–14 October 2016.
33. Law, H.; Deng, J. Cornernet: Detecting objects as paired keypoints. In Proceedings of the European Conference on Computer Vision, Munich, Germany, 8–14 September 2018.
34. Tian, Z.; Shen, C.; Chen, H.; He, T. Fcos: Fully convolutional one-stage object detection. In Proceedings of the IEEE International Conference on Computer Vision, Seoul, Republic of Korea, 27 October–2 November 2019.
35. Carion, N.; Massa, F.; Synnaeve, G.; Usunier, N.; Kirillov, A.; Zagoruyko, S. End-to-end object detection with transformers. In Proceedings of the European Conference on Computer Vision, Glasgow, UK, 23–28 August 2020.
36. Yang, C.; Huang, Z.; Wang, N. QueryDet: Cascaded Sparse Query for Accelerating High-Resolution Small Object Detection. In Proceedings of the IEEE International Conference on Computer Vision and Pattern Recognition, New Orleans, LA, USA, 18–24 June 2022.
37. Zhu, Y.; Zhou, Q.; Liu, N.; Xu, Z.; Ou, Z.; Mou, X.; Tang, J. ScaleKD: Distilling Scale-Aware Knowledge in Small Object Detector. In Proceedings of the IEEE International Conference on Computer Vision and Pattern Recognition, Vancouver, BC, Canada, 17–24 June 2023.
38. Han, W.; Li, J.; Wang, S.; Wang, Y.; Yan, J.; Fan, R.; Zhang, X.; Wang, L. A context-scale-aware detector and a new benchmark for remote sensing small weak object detection in unmanned aerial vehicle images. *Int. J. Appl. Earth Obs. Geoinf.* **2022**, *112*, 102966. [[CrossRef](#)]
39. Cao, B.; Yao, H.; Zhu, P.; Hu, Q. Visible and Clear: Finding Tiny Objects in Difference Map. In Proceedings of the European Conference on Computer Vision, Milan, Italy, 29 September–4 October 2024.

40. Huang, Y.X.; Liu, H.I.; Shuai, H.H.; Cheng, W.H. Dq-detr: Detr with dynamic query for tiny object detection. In Proceedings of the European Conference on Computer Vision, Milan, Italy, 29 September–4 October 2024.
41. Yin, N.; Liu, C.; Tian, R.; Qian, X. SDPDet: Learning Scale-Separated Dynamic Proposals for End-to-End Drone-View Detection. *IEEE Trans. Multimed.* **2024**, *26*, 7812–7822. [\[CrossRef\]](#)
42. Zhang, C.; Liu, T.; Xiao, J.; Lam, K.M.; Wang, Q. Boosting Object Detectors via Strong-Classification Weak-Localization Pretraining in Remote Sensing Imagery. *IEEE Trans. Instrum. Meas.* **2023**, *72*, 1–20. [\[CrossRef\]](#)
43. Zhang, C.; Xiao, J.; Yang, C.; Zhou, J.; Lam, K.M.; Wang, Q. Integrally Mixing Pyramid Representations for Anchor-Free Object Detection in Aerial Imagery. *IEEE Geosci. Remote Sens. Lett.* **2024**, *21*, 1–5. [\[CrossRef\]](#)
44. Duan, C.; Wei, Z.; Zhang, C.; Qu, S.; Wang, H. Coarse-grained density map guided object detection in aerial images. In Proceedings of the IEEE International Conference on Computer Vision Workshops, Montreal, BC, Canada, 11–17 October 2021.
45. Yang, F.; Fan, H.; Chu, P.; Blasch, E.; Ling, H. Clustered object detection in aerial images. In Proceedings of the IEEE International Conference on Computer Vision, Seoul, Republic of Korea, 27 October–2 November 2019.
46. Deng, S.; Li, S.; Xie, K.; Song, W.; Liao, X.; Hao, A.; Qin, H. A Global-Local Self-Adaptive Network for Drone-View Object Detection. *IEEE Trans. Image Process.* **2021**, *30*, 1556–1569. [\[CrossRef\]](#)
47. Meethal, A.; Granger, E.; Pedersoli, M. Cascaded Zoom-In Detector for High Resolution Aerial Images. In Proceedings of the IEEE International Conference on Computer Vision and Pattern Recognition Workshops, Vancouver, BC, Canada, 17–24 June 2023.
48. Liu, C.; Gao, G.; Huang, Z.; Hu, Z.; Liu, Q.; Wang, Y. YOLC: You Only Look Clusters for Tiny Object Detection in Aerial Images. *IEEE Trans. Intell. Transp. Syst.* **2024**, *25*, 13863–13875. [\[CrossRef\]](#)
49. Zhang, C.; Lam, K.M.; Liu, T.; Chan, Y.L.; Wang, Q. Structured Adversarial Self-Supervised Learning for Robust Object Detection in Remote Sensing Images. *IEEE Trans. Geosci. Remote Sens.* **2024**, *62*, 1–20. [\[CrossRef\]](#)
50. Yu, W.; Yang, T.; Chen, C. Towards Resolving the Challenge of Long-Tail Distribution in UAV Images for Object Detection. In Proceedings of the IEEE Winter Conference on Applications of Computer Vision, Waikoloa, HI, USA, 3–8 January 2021.
51. Wang, T.; Li, Y.; Kang, B.; Li, J.; Liew, J.; Tang, S.; Hoi, S.; Feng, J. The devil is in classification: A simple framework for long-tail instance segmentation. In Proceedings of the European Conference on Computer Vision, Glasgow, UK, 23–28 August 2020.
52. Cui, Y.; Jia, M.; Lin, T.Y.; Song, Y.; Belongie, S. Class-balanced loss based on effective number of samples. In Proceedings of the IEEE International Conference on Computer Vision and Pattern Recognition, Long Beach, CA, USA, 15–20 June 2019.
53. Li, Y.; Wang, T.; Kang, B.; Tang, S.; Wang, C.; Li, J.; Feng, J. Overcoming classifier imbalance for long-tail object detection with balanced group softmax. In Proceedings of the IEEE International Conference on Computer Vision and Pattern Recognition, Seattle, WA, USA, 13–19 June 2020.
54. Zhang, S.; Chen, C.; Peng, S. Reconciling Object-Level and Global-Level Objectives for Long-Tail Detection. In Proceedings of the IEEE International Conference on Computer Vision, Paris, France, 1–6 October 2023.
55. Hyun Cho, J.; Krähenbühl, P. Long-tail detection with effective class-margins. In Proceedings of the European Conference on Computer Vision, Tel Aviv, Israel, 23–27 October 2022.
56. Lin, T.Y.; Dollár, P.; Girshick, R.; He, K.; Hariharan, B.; Belongie, S. Feature pyramid networks for object detection. In Proceedings of the IEEE International Conference on Computer Vision and Pattern Recognition, Honolulu, HI, USA, 21–26 July 2017.
57. Bundy, A.; Wallen, L. Breadth-first search. *Cat. Artif. Intell. Tools* **1984**, *1*, 13. [\[CrossRef\]](#)
58. Du, D.; Qi, Y.; Yu, H.; Yang, Y.; Duan, K.; Li, G.; Zhang, W.; Huang, Q.; Tian, Q. The unmanned aerial vehicle benchmark: Object detection and tracking. In Proceedings of the European Conference on Computer Vision, Munich, Germany, 8–14 September 2018.
59. Chen, K.e.a. MMDetection: Open MMLab Detection Toolbox and Benchmark. *arXiv* **2019**, arXiv:1906.07155.
60. Paszke, A.; Gross, S.; Massa, F.; Lerer, A.; Bradbury, J.; Chanan, G.; Killeen, T.; Lin, Z.; Gimelshein, N.; Antiga, L.; et al. Pytorch: An imperative style, high-performance deep learning library. *Adv. Neural Inf. Process. Syst.* **2019**, *32*, 8026–8037.
61. Du, B.; Huang, Y.; Chen, J.; Huang, D. Adaptive Sparse Convolutional Networks With Global Context Enhancement for Faster Object Detection on Drone Images. In Proceedings of the IEEE International Conference on Computer Vision and Pattern Recognition, Vancouver, BC, Canada, 17–24 June 2023.
62. Wei, Z.; Duan, C.; Song, X.; Tian, Y.; Wang, H. Amrnet: Chips augmentation in aerial images object detection. *arXiv* **2020**, arXiv:2009.07168.
63. Zhou, X.; Wang, D.; Krähenbühl, P. Objects as points. *arXiv* **2019**, arXiv:1904.07850.

Disclaimer/Publisher’s Note: The statements, opinions and data contained in all publications are solely those of the individual author(s) and contributor(s) and not of MDPI and/or the editor(s). MDPI and/or the editor(s) disclaim responsibility for any injury to people or property resulting from any ideas, methods, instructions or products referred to in the content.